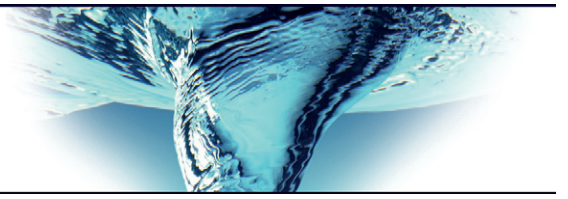
J. Fluid Mech. (2015), *vol.* 764, R2, doi:10.1017/jfm.2014.731



JFM RAPIDS
journals.cambridge.org/rapids

Boundary layer stabilization using free-stream vortices

L. Siconolfi[1], S. Camarri[1] and J. H. M. Fransson[2,†]

[1]Dipartimento di Ingegneria Civile ed Industriale, Università di Pisa, I-561 26 Pisa, Italy

[2]Linné Flow Centre, KTH-Royal Institute of Technology, SE-100 44 Stockholm, Sweden

(Received 8 October 2014; revised 8 December 2014; accepted 16 December 2014;
first published online 30 December 2014)

In this numerical investigation we explore the possibility of applying free-stream vortices as a passive flow control method for delaying the transition to turbulence. The work is motivated by previous experimental studies demonstrating that stable streamwise boundary layer (BL) streaks can attenuate both two- and three-dimensional disturbances inside the BL, leading to transition delay, with the implication of reducing skin-friction drag. To date, successful control has been obtained using physical BL modulators mounted on the surface in order to generate stable streaks. However, surface mounted BL modulators are doomed to failure when the BL is subject to free-stream turbulence (FST), since a destructive interaction between the two is inevitable. In order to tackle free-stream disturbances, such as FST, a smooth surface is desired, which has motivated us to seek new methods to induce streamwise streaks inside the BL. A first step, in a systematic order, is taken in the present paper to prove the control idea of generating free-stream vortices for the attenuation of ordinary Tollmien–Schlichting waves inside the BL. In this proof-of-concept study we show that, by applying a spanwise array of counter-rotating free-stream vortices, inducing streamwise BL streaks further downstream, it is possible to alter the BL stability characteristics to such a degree that transition delay may be accomplished. For the demonstration we use direct numerical simulations along with stability analysis.

Key words: boundary layer control, drag reduction, transition to turbulence

1. Introduction

Delay of the laminar–turbulent transition in a boundary layer (BL) has been a subject of great interest over several decades, due to its benefits in terms of reduced skin friction as well as heat transfer to the surface in many real flow applications. The prototype flow for this kind of investigation is the Blasius BL developing on a

† Email address for correspondence: jens.fransson@mech.kth.se

© Cambridge University Press 2014

https://doi.org/10.1017/jfm.2014.731 Published online by Cambridge University Press

flat plate. In this case, for low-intensity external disturbances the transition scenario is dominated by exponentially growing plane waves, known as Tollmien–Schlichting (TS) waves. It has been shown that TS waves can be attenuated by properly shaped and stable spanwise velocity modulations inside the BL, denoted as streaks, thus leading to transition delay. The streaks are high- and low-speed regions in the BL generated by a convective mechanism transporting fluid with high momentum close to the wall and ejecting low-momentum fluid in the outer region of the BL. This process is usually referred to as the lift-up mechanism (Landahl 1980).

To the best of the authors' knowledge, the first experimental evidence of stabilization of TS waves by streamwise streaks is reported in Kachanov & Tararykin (1987). Theoretical support has been given in Cossu & Brandt (2002, 2004) by direct numerical simulation (DNS) and local temporal stability analysis. In the experiments by Fransson *et al.* (2004, 2005, 2006), streamwise BL streaks were generated using circular roughness elements, and it was shown that higher streak amplitudes improved the stabilization up to a certain threshold streak amplitude, above which a rapid transition took place triggered by a shedding mode at the location of the roughness elements. In order to increase the maximum amplitude of the stable streaks, which is limited to 12 % of the free-stream velocity (U_∞) using circular roughness elements, Fransson & Talamelli (2012) proposed to employ small winglet pairs periodically distributed in the spanwise direction, denoted miniature vortex generators (MVGs). It was shown experimentally that MVGs can generate stable streaks with maximum amplitudes of up to 32 % of U_∞. The MVGs generate streamwise vortices, which modulate the BL and form velocity streaks by the lift-up mechanism. The streamwise decay of the streaks can be quite rapid, since the generated vortices lie inside the BL where viscous effects are important. To overcome this problem, Fransson & Talamelli (2012) proposed the use of multiple MVG arrays distributed in the streamwise direction so as to regenerate the streaks and to extend the stabilizing effect further downstream. The possibility of delaying transition and accomplishing net skin-friction drag reduction of at least 65 % using MVGs has been investigated experimentally and is reported in Shahinfar *et al.* (2012, 2013), Shahinfar, Sattarzadeh & Fransson (2014) and Sattarzadeh *et al.* (2014).

In order to avoid the installation of devices inside the BL, which can be detrimental for stability in off-design flow conditions, and to create streaks with a strong persistency in the streamwise direction, it would be advantageous if MVGs or similar devices generating streamwise vortices could be placed outside the BL. In this way, it would be possible to relax the limitations due to the scaling with the BL thickness, decrease viscous damping and avoid geometric discontinuities in the BL. These considerations motivate the present work, which is dedicated to numerical investigation of the generation of velocity streaks by using the lift-up mechanism through free-stream vortices, which penetrate the BL further downstream, and to characterization of the effect of the generated streaks on the stability of the BL itself. The work is inspired by the experiment documented in Tani & Komoda (1962), where small-amplitude streamwise streaks ($\simeq$6 % of U_∞) were produced with a series of small wings placed outside the BL. In the present work we do not focus on the design of a specific device to generate free-stream vortices, as for instance the winglets used in Tani & Komoda (1962); instead, we directly simulate the evolution of modelled vortices in the flow. This has been carried out by varying the free parameters of the flow configuration in a range of realistic values according to our previous experience with the DNS of the flow past MVGs (Camarri, Fransson & Talamelli 2013), but without parameter optimization. Our result is a proof of

https://doi.org/10.1017/jfm.2014.731 Published online by Cambridge University Press

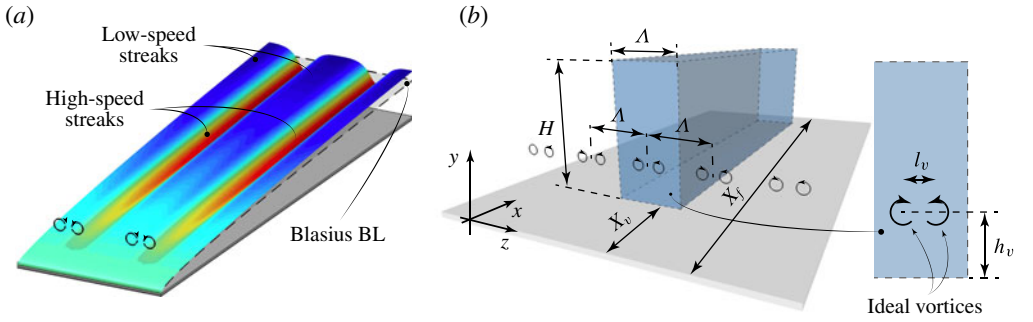


FIGURE 1. (*a*) Sketch of flow configuration illustrating the modulation of the BL by the free-stream vortices; (*b*) the computational box with some of the free parameters defined in the text.

concept that it is possible to identify configurations of free-stream vortices, which show very promising characteristics and hence will be worth testing experimentally with free-stream turbulence. Among the tested configurations, two are selected and investigated in more detail here.

2. Flow configuration

A sketch of the considered flow configuration is shown in figure 1, with modelled free-stream vortices being introduced at a given distance from the plate leading edge (X_v). The vortices are placed outside the BL at a distance h_v from the wall and have a radius r_0 of the same order of magnitude as the BL thickness. The spanwise periodicity of the vortex pairs is denoted by the spanwise wavelength Λ (m), i.e. the distance between two neighbouring vortex pairs. Two different vortex models have been used to approximate the vorticity inside each single vortex, namely the Rankine and Batchelor vortex models (see Batchelor 1964). In both models the vortices are assumed to be perfectly circular with total circulation Γ_0. In the Rankine model the axial vorticity is uniform inside the cores, so that the induced velocity field is tangential to the core and its intensity increases linearly inside the core and decreases as $1/r$ outside, r being the distance from the vortex centre. In the Batchelor vortex adopted here (Velte, Hansen & Okulov 2008) the induced velocity has both a tangential (v_θ) and an axial (v_x) component:

$$v_\theta(r,\theta) = \frac{\Gamma}{2\pi r}\left[1-\exp\left(-\frac{r^2}{r_0^2}\right)\right], \quad v_x(r,\theta) = -\frac{\Gamma}{2\pi l_p}\left[\exp\left(-\frac{r^2}{r_0^2}\right)\right], \qquad (2.1a,b)$$

where l_p is the helical pitch of the vortex, which determines the velocity defect in the streamwise direction. In order to choose reasonable ranges to vary the free parameters of the considered flow configuration we have selected a successful experimental set-up, namely the C01 case documented in Shahinfar *et al.* (2013), as guidance. The vortices, inducing streaks in the C01 case, were generated using MVGs mounted on the surface and have been studied in detail using DNS (Camarri *et al.* 2013), which makes this case suitable. In C01 the fluid was air at atmospheric conditions, the free-stream velocity was $U_\infty = 7.7$ m s^{-1}, the kinematic viscosity was $\nu = 1.46 \times 10^{-5}$ m^2 s^{-1}, the height of the MVGs was 1.3 mm and they were installed 222 mm downstream of the leading edge of the plate. In the present paper we consider the same flow

https://doi.org/10.1017/jfm.2014.731 Published online by Cambridge University Press

parameters U_∞ and ν, and our results are sometimes shown in dimensional form to facilitate the comparison with the experimental C01 case.

3. Numerical set-up

3.1. *Direct numerical simulations*

The numerical code used for the DNS is NEK5000, an open-source massively parallel spectral element code. The spatial discretization is based on a local tensor product of Gauss–Lobatto–Legendre quadrature points within each hexahedral element. Pressure stabilization is obtained by a P_N–P_{N-2} formulation (in the present simulations $N \geqslant 9$). A third-order backward-differentiation formula in time is used for the time derivatives. Concerning the other terms of the equations, the viscous ones are treated implicitly while the nonlinear convective ones are forward extrapolated in time with third-order accuracy so as to treat them explicitly in the time-advancing scheme. Details on the code can be found following the link http://nek5000.mcs.anl.gov/index.php/Main_Page.

The simulations of the steady BL flow including the free-stream vortices were carried out with a computational domain starting at X_v, which is a variable in the range $0 \leqslant Re_{X_v} = X_v U_\infty/\nu \leqslant 2.74 \times 10^4$, where Re_{X_v} is the Reynolds number at X_v and ending at X_f. The height of the computational domain is $H = 86$ mm, giving $H/\delta \geqslant 274$ at the inlet section where $\delta(x) = \sqrt{\nu x/U_\infty}$ is the characteristic length scale of the BL. The simulations are limited to computing only one pair of free-stream vortices, i.e. with a spanwise computational domain width of 1Λ, but with the imposition of periodic boundary conditions in the spanwise direction. Two different streamwise extents of the computational domains were used: the first domain (D1) extends for a normalized length equal to $\Delta Re_X = Re_{X_f} - Re_{X_v} \simeq 4.24 \times 10^5$ and employs approximately 6×10^7 degrees of freedom (dofs); the second one (D2), used for the configurations of slowly evolving streaks, has $\Delta Re_X = Re_{X_f} - Re_{X_v} \simeq 1.00 \times 10^6$ with approximately 10^8 dofs.

The imposed velocity distribution at the inflow at X_v consists of a superposition of the velocity field induced by a pair of vortices in the free stream to a Blasius BL profile. This implies that the axis of the vortices at X_v is parallel with the plate. No-slip boundary conditions are used at the solid wall and null-stress outflow boundary conditions are imposed on the outflow and on the top boundary. The spatial resolution has been chosen on the basis of the simulations reported in Camarri *et al.* (2013) and of dedicated convergence tests which are not shown here for the sake of brevity. Moreover, the results of the DNS have been further validated against those obtained by a three-dimensional BL solver and employing a completely different numerics (mixed finite-difference/finite-element discretization on unstructured grid).

Simulations of transition, triggered by forcing high-initial-amplitude TS waves, have also been performed in order to investigate the control effect by the free-stream vortices on transition delay. In these simulations the domain was extended to 10Λ in the spanwise direction, thus including 10 pairs of counter-rotating vortices to avoid any influence of the boundary conditions on the transition location. In the streamwise direction the domain extends from $Re_{X_v} = 5.28 \times 10^4$ to $Re_{X_f} = 6.11 \times 10^5$ and the normalized forcing frequency of the TS wave is $F = 10^6(2\pi f \nu/U^2) = 140$. The TS waves are excited in the DNS by a time-periodic volume force oriented in the wall-normal direction and acting in a narrow streamwise strip centred at the point $X_{TS} = 150$ mm. The forcing frequency matches the experimental C01 case and the wall-normal disturbance amplitude further downstream compares well with the corresponding eigenfunction of the Orr–Sommerfeld equation. The adopted boundary

https://doi.org/10.1017/jfm.2014.731 Published online by Cambridge University Press

conditions are the same as for the simulation of the base flow. Concerning the spatial discretization, convergence tests have been carried out leading to a grid that is globally coarser than the one used for a single vortex pair and employs approximately 2×10^8 dofs. This grid regeneration was carried out because of the different streamwise extension of the domain for the transition simulations and, at the same time, in order to keep the number of dofs for the transition simulation affordable from a computational point of view.

3.2. *Biglobal stability analysis*

The linear stability of the streaky BL induced by the free-stream vortices has been characterized by performing a local biglobal stability analysis, similar to the analysis by Piot, Casalis & Rist (2008) on the flow past a periodic row of roughness elements. Since the flow is fully three-dimensional, the discretization of the stability problem has to be performed in the cross-sectional yz-plane at each downstream location. The local stability problem is governed by the linearized Navier–Stokes equations for an incompressible flow and a generic solution of the streamwise (u), wall-normal (v) and spanwise (w) velocity disturbances as well as the pressure perturbation (p) is searched for in the following modal form: $\{u, v, w, p\} = \{\tilde{u}, \tilde{v}, \tilde{w}, \tilde{p}\}(y, z)\mathrm{e}^{\mathrm{i}(\alpha x - \omega t)}$. Here, $\tilde{}$ denotes the disturbance amplitude distribution in the yz-plane, α is the streamwise wavenumber and ω is the angular frequency. The disturbance is assumed to vanish on and far away from the wall, and to be periodic in the spanwise direction (subharmonic modes have also been checked using multiples of the periodicity length of the base flow). When the linearized Navier–Stokes equations are discretized in space, a generalized eigenvalue problem is obtained, which is quadratic in α for the spatial analysis (ω fixed) and linear in ω for the temporal analysis (α fixed). Spatial discretization is here obtained by a finite-element formulation on unstructured grids, employing Taylor–Hood elements. The open-source code FreeFem++ (http://www.freefem.org) has been used to this purpose. The stability has been characterized by a spatial stability analysis. The initial guess for the solution of the resulting nonlinear eigenvalue problem has been estimated by performing a temporal stability analysis and applying the Gaster transformation to the results. Both the linear and nonlinear eigenvalue problems have been solved by a Krylov–Schur method with a shift-invert technique, using the parallel implementation available in the SLEPc library (see http://www.grycap.upv.es/slepc/).

4. Results and discussion

4.1. *Exploration of the free parameters*

In the present flow configuration there are a number of free parameters, as detailed in § 2 and illustrated in figure 1. The geometrical and vortical parameters are (X_v, h_v, l_v, Λ) and (r_0, Γ_0, l_p) respectively, with l_p only being part of the Batchelor vortex model. As already discussed, we intend to demonstrate the use of free-stream vortices for BL flow control, and hence an optimization of all the above parameters is beyond the scope of the present study. However, since modelled vortices are introduced it is important to grant the physical realizability of the flow by varying the free parameters within physically meaningful ranges. These have been determined on the basis of previous experience with MVGs, as described below.

Physically relevant values of r_0, Γ_0 and l_v have been found by analysing the vorticity generated past the MVGs in case C01 (see Shahinfar *et al.* 2013), which has been extracted from available DNS data (Camarri *et al.* 2013). The streamwise

https://doi.org/10.1017/jfm.2014.731 Published online by Cambridge University Press

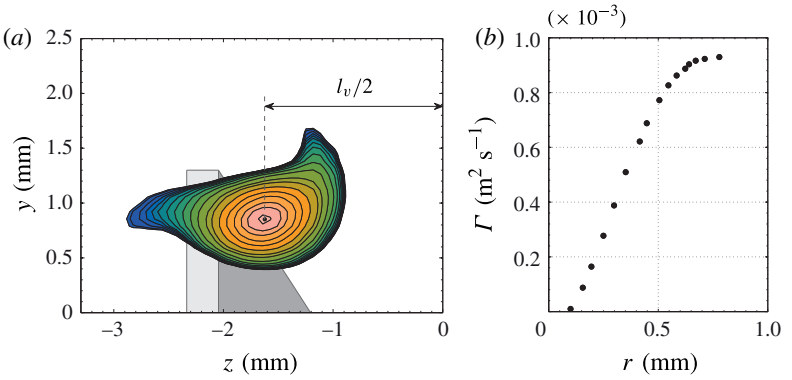


FIGURE 2. (*a*) Streamwise vorticity in the vortex 13 mm behind one MVG blade (shown in the background) for configuration C01 (isocontours equally distributed from 0 to 1.0×10^{-3} m^2 s^{-1}). (*b*) Vortex circulation, computed on the isocontours of vorticity, plotted against the area-weighted mean radius r.

vorticity distribution inside one of the two counter-rotating vortices past an MVG pair is shown in figure 2(*a*) at a distance of 13 mm downstream of the MVG. The circulation has been calculated on circuits coinciding with the isocontours of axial vorticity (in figure 2*a*) and is plotted in figure 2(*b*) versus the averaged distance r of each isocontour from the centre of the vortex. Plausible values for (r_0, l_v, Γ_0) have been derived to be (0.8 mm, 3.12 mm, 9×10^{-4} m^2 s^{-1}) respectively from the synthetic data in figure 2(*a,b*). The parameters $l_v = 3.12$ mm and $\Lambda = 13$ mm have been kept constant for all cases. We note that the only parameters that cannot be extracted on the basis of case C01 are X_v and h_v, since they are related to the placement of a hypothetical free-stream device generating the vortices. However, a constraint on h_v is that we are interested in generating the vortices outside the BL and X_v should be chosen such that an appreciable streak amplitude is obtained in the region of convective instability for the uncontrolled BL.

On the basis of the above considerations an exploratory set of simulations, varying some of the free parameters in the ranges ($0.65 \leqslant r_0 \leqslant 1.3$) mm, ($1.30 \leqslant H \leqslant 7.80$) mm, ($0 \leqslant X_v \leqslant 235.00$) mm and ($6 \times 10^{-4} \leqslant \Gamma_0 \leqslant 27 \times 10^{-4}$) m^2 s^{-1}, were carried out in domain D1. A representative subset of the obtained results, using the Rankine model for the inlet conditions, is reported in figure 3, where the conventional streak amplitude measure,

$$A_{ST}^{max} = \max_y \left[\max_z \{U(X, y, z)\} - \min_z \{U(X, y, z)\} \right] \Big/ (2U_\infty), \tag{4.1}$$

is plotted versus x. Figure 3(*a*) illustrates the effect of h_v on the generated streaks ($X_v = 26.0$ mm). The three values $h_v = 1.95$, 2.60, 3.90 mm correspond to $h_v/\delta(X_v) = 8.8$, 11.7, 17.6 respectively. It should be recalled that the Blasius BL edge corresponds to approximately 5δ. As h_v increases, the global A_{ST}^{max} maximum increases slightly, but with its corresponding downstream position appearing further downstream. This is an expected behaviour, since the further away from the BL edge the vortices are, the lower the dissipation rate becomes, and at the same time they induce a smaller modulation of the BL. The effect on the streak amplitude evolution by varying X_v is rather weak, as illustrated in figure 3(*b*). It is worth noting that a variation in X_v

https://doi.org/10.1017/jfm.2014.731 Published online by Cambridge University Press

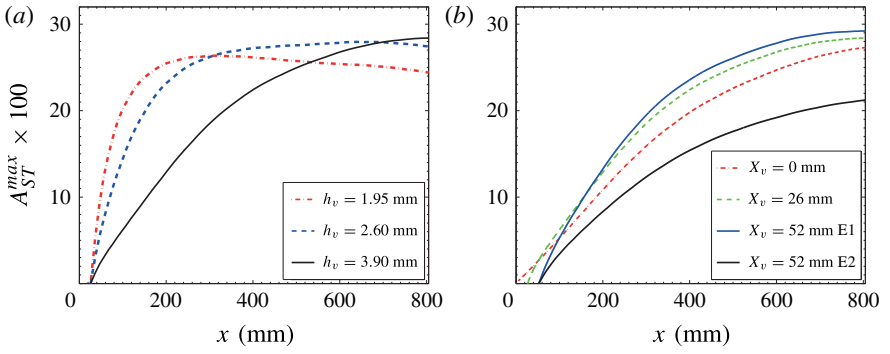


FIGURE 3. Streamwise evolution of the streak amplitude on varying (*a*) h_v ($X_v = 26$ mm) and (*b*) X_v ($h_v = 3.90$ mm). The Rankine vortex model is used here.

brings approximately a variation of $h_v/\delta(X_v)$ for a constant h_v, which may explain the variations among the cases in figure 3(*b*). In the same figure, two different Γ-values are also considered, namely 6×10^{-4} (case E1) and 9×10^{-4} m^2 s^{-1} (case E2), plotted with blue and black lines respectively. As expected, the evolution of the streak amplitude is quite similar but with a lower amplitude for a lower Γ-value. From here on, we will focus on these two cases (E1 and E2) with the parameters E1: $X_v = 52$ mm, $r_0 = 1.3$ mm, $h_v = 3.9$ mm (or $h_v/\delta(X_v) = 12.5$) and $\Gamma_0 = 9 \times 10^{-4}$ m^2 s^{-1}; E2: as E1 but with $\Gamma_0 = 6 \times 10^{-4}$ m^2 s^{-1}. Case E2 has been designed to obtain a global A_{ST}^{max} maximum approximately equal to that in C01, which has proven to successfully attenuate TS waves and accomplish transition delay.

Finally, as concerns the sensitivity to the actual vortex model, case E1 was also computed using the Batchelor model (case E1b). In this case the helical pitch l_p was set to 2.6 mm, in agreement with the experimental results in Velte *et al.* (2008), where a similar configuration to ours was investigated. The results for E1b (discussed later in figure 5*a*) show that the difference in streak amplitude with respect to the two different vortex models (Rankine and Batchelor) corresponds to a maximum of 2 percentage units in terms of the global A_{ST}^{max} maximum. Thus, we can conclude that the streamwise amplitude evolution is rather insensitive to the selected vortex model.

4.2. *Streamwise evolution of streaks*

Three downstream locations of the streamwise velocity (colourmap) together with the streamwise vortices, identified using isocontours of the λ_2 vortex identification criterion, are shown in figure 4 for the E2 case. The three plots clearly show that the streamwise vortices successively modulate the BL in the streamwise direction. These vortices drive high-momentum fluid from the free stream towards the wall in between the two vortices of a pair, while low-momentum fluid is elevated in the region between two contiguous vortex pairs. Since $l_v < \Lambda$, the resulting high-velocity streaks are initially narrower and stronger than the low-velocity streaks. Moving downstream along the plate, the streamwise vortices progressively approach and eventually enter the BL.

In figure 5(*a*) the experimental A_{ST}^{max} for case C01 is plotted and compared with the induced BL streak amplitude by the free-stream vortices (E1 and E2 cases). This shows that when MVGs are used, the BL streaks are formed markedly earlier since the vortices are intense and already inside the BL, but the streaks also dissipate

https://doi.org/10.1017/jfm.2014.731 Published online by Cambridge University Press

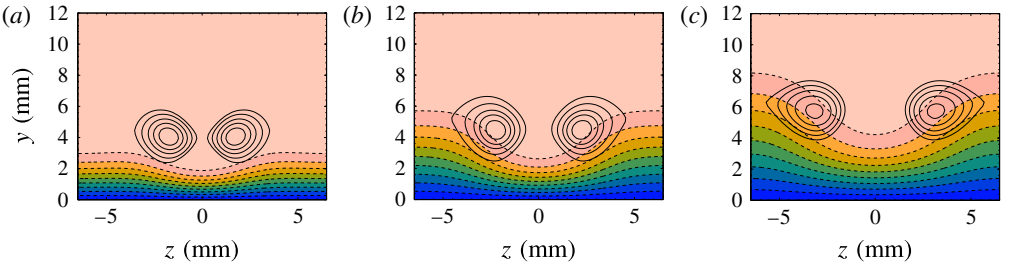


FIGURE 4. Case E2: cross-sectional contours of the mean streamwise velocity field U/U_∞: (*a*) $x = 310$ mm, (*b*) $x = 850$ mm and (*c*) $x = 1675$ mm. The dashed black lines are contours of constant velocity (0.1:0.1:0.9). The solid black lines represent the λ_2 vortex identification criterion.

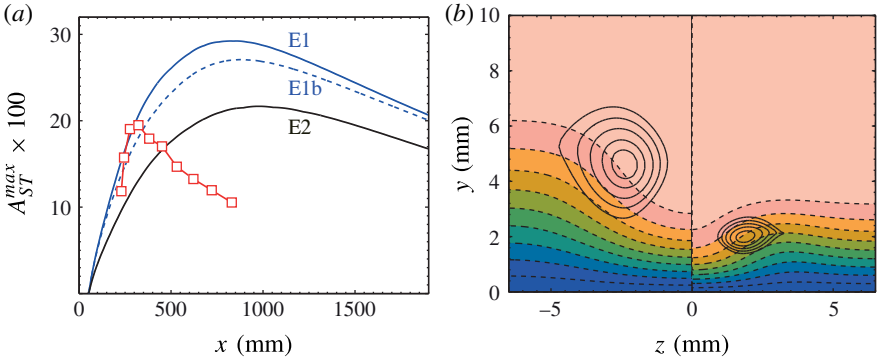


FIGURE 5. (*a*) Streamwise streak amplitude evolution for the cases C01 (□, from experiments), E1 (blue line), E1b (dashed line) and E2 (black line). (*b*) Cross-sectional contours of normalized mean streamwise velocity U/U_∞, for E2 (left) and for C01 (DNS, right) at the position of global streak amplitude maximum. Dashed contour lines correspond to (0.1:0.1:0.9). The solid black lines represent the λ_2 vortex identification criterion.

more rapidly. When vortices equivalent to those past the MVGs are positioned outside the BL (case E1), they generate higher-amplitude streaks because the lift-up mechanism is active for a longer distance. This is quantified in figure 6(*a*), where a significantly more rapid decay of vortex circulation for the BL vortices is shown compared with the free-stream vortex decay of the E1 and E2 cases. Since the induced velocity modulations are initially weaker due to the longer distance from the wall, the generation process takes a longer streamwise distance to reach the same amplitude. Thus, to obtain a global A_{ST}^{max} maximum equal to that in case C01, less intense vortices should be used, as in case E2. An additional comparison between the cases E2 and C01 is shown in figure 5(*b*), where the streamwise velocity and the streamwise vortices of E2 (left) and C01 (right) are reported at the point of global A_{ST}^{max} maximum of both cases. The figure clearly highlights the differences between the two cases, especially in the shape of the velocity streaks and the different positions of the streamwise vortex within the BL.

https://doi.org/10.1017/jfm.2014.731 Published online by Cambridge University Press

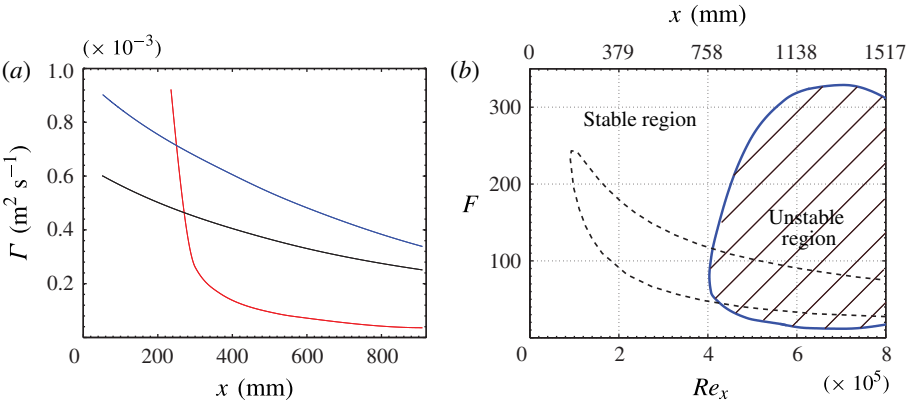


FIGURE 6. (*a*) Streamwise evolution of the circulation of the streamwise vortices for E1 (blue line), E2 (black line) and C01 (DNS, red line). (*b*) The solid blue line corresponds to the neutral curve for E1 and the dashed line to the neutral curve for the Blasius BL in the F–Re-plane. Case E2 is stable in the range of Re_x considered in the figure.

4.3. *Spatial stability analysis*

Here, we present the results of the biglobal spatial stability analysis of the cases E1 and E2. The results are condensed in the F–Re stability diagram shown in figure 6(*b*), where the solid blue line enclosing the striped area corresponds to the E1 case and the dashed line to the neutral stability curve of the reference Blasius BL. For the E1 case the unstable region is enlarged, with respect to the Blasius BL, in terms of a broader frequency range, but with a downstream shift of the critical Reynolds number (Re_x^{cr}) down to $Re_x^{cr} \approx 4 \times 10^5$, i.e. delayed by a factor of four. Inside the unstable region (striped area) the growth factors for both cases are comparable (not shown in the figure), indicating that the E1 streaky base flow case has the potential to accomplish transition delay with respect to the Blasius BL. The onset of instability of the E1 case starts around the streamwise position where the global A_{ST}^{max} maximum is located (see figure 5). With the current knowledge on streamwise streak instability we suspect that the instability in the E1 case, with a global A_{ST}^{max} maximum of approximately 29 % of U_∞, is driven by an instability of the streaks themselves, whose amplitude is too high.

For the E2 case, on the other hand, the modulated BL is stable for all the sections of the computational domain, i.e. the critical Reynolds number is greater than $Re_x^{cr} = 8 \times 10^5$. With a global A_{ST}^{max} maximum of less than 22 % of U_∞, it is close to the successful experimental case C01 and well below the critical A_{ST}^{max} of 26 % of U_∞ for the onset of sinusoidal secondary instability (see Andersson *et al.* 2001). This explains why in E2, where the streak amplitude is lower, the convective instability of the BL is completely stabilized throughout the length of the computational domain.

The results presented here demonstrate that there is a large margin of improvement for the stability of the controlled BL, since it is possible to modify the streak amplitude and its shape by acting on several parameters. For instance, the amplitude of the generated streaks can be controlled both by acting on Γ, as done in switching from E1 to E2, and by varying the initial distance h_v of the vortices from the wall, so as to reduce the intensity of the induced velocities at the BL edge by the lift-up mechanism. Despite this the free parameters are not optimized, that is with the present

https://doi.org/10.1017/jfm.2014.731 Published online by Cambridge University Press

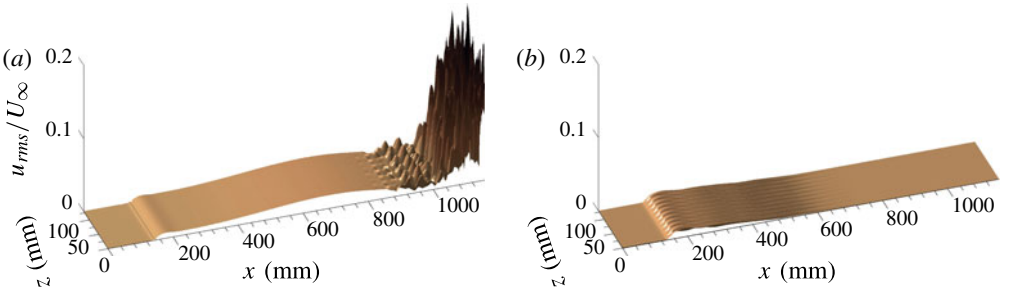


FIGURE 7. Dimensionless temporal root mean square streamwise velocity fluctuations u_{rms}/U_∞ in the xz-plane at $y = 1.0$ mm (TS waves at $F \simeq 140$): (a) without free-stream vortices; (b) with free-stream vortices (case E1).

configurations E1 and E2, the delay in the onset of convective instability inside the BL is so evident that a gain in terms of transition delay is expected by the proposed control.

4.4. *BL transition delay*

Previously reported experiments (Shahinfar *et al.* 2013) and now DNS simulations have been carried out for the configuration C01, where transition was triggered by forcing a TS wave at $F \simeq 140$. This frequency was chosen in the experiment after having locked the location of the MVG array and successfully established a stable streaky BL. The desire was to locate branch I of the neutral stability curve of the reference Blasius BL without the MVGs at the location of the global A_{ST}^{max} maximum, which has shown to be effective in attenuating TS waves (see Bagheri & Hanifi 2007). In the DNS documented here the TS waves are forced as detailed in § 3 at $F = 140.6$. The forcing has been introduced in a DNS simulation of the reference Blasius BL, and the forcing amplitude has been varied and tuned so as to observe transition inside the computational domain. The result is shown in figure 7(a), where the temporal root mean square fluctuations of the normalized streamwise velocity (u_{rms}/U_∞) are plotted in the xz-plane 1 mm above the wall. The figure shows that the initially forced amplitude at $X_{TS} = 150$ mm decays until it reaches branch I ($x \approx 250$ mm), from where the u_{rms} starts to grow, which it does beyond branch II ($x \approx 600$ mm) since the flow is no longer linear with this high forcing amplitude. After some downstream location the u_{rms} level decreases slightly, whereafter the flow undergoes a secondary instability, triggering transition after $x \simeq 850$ mm. In a second DNS simulation the same forcing was applied as in the Blasius BL, but with the presence of the free-stream vortices (case E1). The result is presented in figure 7(b), showing that the disturbance is rapidly attenuated after an initial transient growth. The forced TS waves reach such a low value that it is not possible to detect any successive growth, at the scale of the plot, when they again enter the convectively unstable region, which is almost at the end of the computational domain (recall that $Re_{X_f} = 6.11 \times 10^5$).

The test carried out in the present section shows that, even though it is the E1 case that is considered, which is characterized by the stability curve illustrated in figure 6(b), it is possible to obtain an evident transition delay with respect to the reference Blasius BL. A DNS with TS wave forcing of the E2 case has not been carried out here, but an even better result is expected since the onset of convective instability in the BL is even further delayed compared with the E1 case (see figure 6b).

https://doi.org/10.1017/jfm.2014.731 Published online by Cambridge University Press

5. Summary

In this proof-of-concept study, we show that proper free-stream vortices can stabilize a BL by modulating it as they are convected downstream. The modulation is realized by the lift-up mechanism induced by the vortices, which leads to the formation of steady and stable BL streaks, and the resulting stabilizing effect is attributed to the mechanism of spanwise mean velocity gradients. This way of introducing steady streamwise streaks to accomplish transition delay, with the implication of reducing skin-friction drag, has not been reported previously. Despite the absence of an optimization procedure of the free parameters, instead simply exploring physically relevant values, an evident transition delay has been obtained. It is hypothesized that the present control idea is also better suited than surface mounted BL modulators to tackling the challenge of FST as an external disturbance source.

Acknowledgements

The authors wish to acknowledge PRACE for awarding access to the resource Fermi based in Italy at Cineca. J.H.M.F. acknowledges the European Research Council for their financial support of the AFRODITE project through a Starting Independent Researcher Grant. S.C. acknowledges travelling support by the 'C.M. Lerici' Foundation.

References

ANDERSSON, P., BRANDT, L., BOTTARO, A. & HENNINGSON, D. S. 2001 On the breakdown of boundary layer streaks. *J. Fluid Mech.* **428**, 29–60.

BAGHERI, S. & HANIFI, A. 2007 The stabilizing effect of streaks on TS and oblique waves: a parametric study. *Phys. Fluids* **19**, 078103.

BATCHELOR, G. K. 1964 Axial flow in trailing line vortices. *J. Fluid Mech.* **20**, 645–658.

CAMARRI, S., FRANSSON, J. H. M. & TALAMELLI, A. 2013 Numerical investigation of the Afrodite transition control strategy. In *Progress in Turbulence V* (ed. A. Talamelli, M. Oberlack & J. Peinke), pp. 65–69. Springer.

COSSU, C. & BRANDT, L. 2002 Stabilization of Tollmien–Schlichting waves by finite amplitude optimal streaks in the Blasius boundary layer. *Phys. Fluids* **14**, L57–L60.

COSSU, C. & BRANDT, L. 2004 On Tollmien–Schlichting-like waves in streaky boundary layers. *Eur. J. Mech. (*B*/Fluids)* **23**, 815–833.

FRANSSON, J. H. M., BRANDT, L., TALAMELLI, A. & COSSU, C. 2004 Experimental and theoretical investigation of the nonmodal growth of steady streaks in a flat plate boundary layer. *Phys. Fluids* **16** (10), 3627–3638.

FRANSSON, J. H. M., BRANDT, L., TALAMELLI, A. & COSSU, C. 2005 Experimental study of the stabilisation of Tollmien–Schlichting waves by finite amplitude streaks. *Phys. Fluids* **17**, 054110.

FRANSSON, J. H. M. & TALAMELLI, A. 2012 On the generation of steady streamwise streaks in flat-plate boundary layers. *J. Fluid Mech.* **698**, 211–234.

FRANSSON, J. H. M., TALAMELLI, A., BRANDT, L. & COSSU, C. 2006 Delaying transition to turbulence by a passive mechanism. *Phys. Rev. Lett.* **96**, 064501.

KACHANOV, Y. S. & TARARYKIN, O. I. 1987 Experimental investigation of a relaxing boundary layer. *Proc. Siberian Div. USSR Acad. Sci., Ser. Tech. Sci.* **18** (5), 9–19 (in Russian).

LANDAHL, M. T. 1980 A note on an algebraic instability of inviscid parallel shear flows. *J. Fluid Mech.* **98**, 243–251.

PIOT, E., CASALIS, G. & RIST, U. 2008 Stability of the laminar boundary layer flow encountering a row of roughness elements: biglobal stability approach and DNS. *Eur. J. Mech.* B **27**, 684–706.

https://doi.org/10.1017/jfm.2014.731 Published online by Cambridge University Press

SATTARZADEH, S. S., FRANSSON, J. H. M., TALAMELLI, A. & FALLENIUS, B. E. G. 2014 Consecutive turbulence transition delay with reinforced passive control. *Phys. Rev.* E **89**, 061001(R).

SHAHINFAR, S., FRANSSON, J. H. M., SATTARZADEH, S. S. & TALAMELLI, A. 2013 Scaling of streamwise boundary layer streaks and their ability to reduce skin-friction drag. *J. Fluid Mech.* **733**, 1–32.

SHAHINFAR, S., SATTARZADEH, S. S. & FRANSSON, J. H. M. 2014 Passive boundary layer control of oblique disturbances by finite-amplitude streaks. *J. Fluid Mech.* **749**, 1–36.

SHAHINFAR, S., SATTARZADEH, S. S., FRANSSON, J. H. M. & TALAMELLI, A. 2012 Revival of classical vortex generators now for transition delay. *Phys. Rev. Lett.* **109**, 074501.

TANI, I. & KOMODA, H. 1962 Boundary layer transition in the presence of streamwise vortices. *J. Aero. Sci.* **29**, 440–444.

VELTE, C. M., HANSEN, M. O. L. & OKULOV, V. L. 2008 Helical structure of longitudinal vortices embedded in turbulent wall-bounded flow. *J. Fluid Mech.* **619**, 167–177.

https://doi.org/10.1017/jfm.2014.731 Published online by Cambridge University Press